Quantum Dissipative Continuous Time Crystals

Felix Russo* and Thomas Pohl†
Institute for Theoretical Physics, Vienna University of Technology (TU Wien), Vienna, Austria

(Received 2 April 2025; accepted 8 August 2025; published 11 September 2025)

Continuous time crystals, i.e., nonequilibrium phases with a spontaneously broken continuous time-translational symmetry, have been studied and recently observed in the long time dynamics of open quantum systems. Here, we investigate a lattice of interacting three-level particles and find two distinct time-crystal phases that cannot be described within mean-field theory. Remarkably, one of them emerges only in the presence of correlations, upon accounting for beyond-mean-field effects. Our findings extend explorations of continuous time-translational symmetry breaking in dissipative systems beyond the classical phenomenology of periodic orbits in a low-dimensional nonlinear system. The proposed model applies directly to the laser-driven dynamics of interacting Rydberg states in neutral-atom arrays and suggests that the predicted time-crystal phases are observable in such experiments.

DOI: 10.1103/dc2s-94gv

The concept of symmetry breaking is instrumental in understanding a broad range of fundamental processes in physics, chemistry, and biology [1]. Among the most ubiquitous examples is the emergence of ordered structures from an otherwise homogeneous system. In recent years, the question of whether translational symmetry could be broken in the fourth dimension has attracted much attention [2–5]. A quantum system that self-organizes in time, i.e., a time crystal, represents a new exotic state of matter. Early theoretical work focused on discrete time-translational symmetry breaking in periodically driven systems [6–8], which has subsequently been observed in different experimental platforms [9–17]. For time-independent systems, the possibility of continuous time-translational symmetry breaking was pointed out in [18] in the form of a so-called boundary time crystal, where a fraction of a many-body system can undergo spontaneous oscillations. The emergence of a continuous time-crystal (CTC) phase in this setting is directly connected to the physics of dissipative quantum systems, which can exhibit limit-cycle solutions [18–21] that were recently observed experimentally in nonlinear optical cavities [22,23], optical metamaterials [24], thermal Rydberg vapors [25,26], and semiconductors [27].

Despite the diversity of physical platforms and models, an overarching question has been whether time-translational symmetry breaking can be understood classically and to what extent quantum mechanics determines the properties of time-crystal phases [18,21,28–32]. In current experiments and theoretical models, the emergence of CTC phases in dissipative quantum many-body systems is largely understood in terms of a mean-field picture. Hereby, the dynamics of single-particle observables are governed by a small set of nonlinear equations of motion that can exhibit limit-cycle attractors. In fact, the emergence of persistent oscillations in open quantum systems can be associated with an approach to the classical limit [33], while quantum-mechanical extensions of mean-field models have been found to cause damping of limit cycles [28,34]. Hence, there is currently no experimental or theoretical evidence for continuous quantum time-crystal (qCTC) phases in open quantum systems that do not pertain to the limit-cycle phenomenology of nonlinear mean-field equations.

Here, we address this question by exploring the dissipative dynamics of a spin-1 lattice with finite-range interactions that do not afford an exact mean-field description. Numerical simulations reveal two distinct time-crystalline phases with persistent oscillations of all observables in the thermodynamic limit. The first kind is found under conditions for which limit-cycle dynamics are predicted by mean-field theory but survive in the presence of significant quantum fluctuations. In addition, we identify a second type of qCTC that is not predicted by mean-field theory but instead is driven by correlations. This phase features a distinct scaling of quantum fluctuations with system size and emerges in the absence of long-range order, consistent with the phenomenology of oscillatory solutions in quenched isolated quantum systems [35]. The found qCTC phases do not rely on symmetries of the underlying master equation and are robust to perturbations, both of which are essential aspects for potential experiments. Indeed, the studied model and considered parameters for qCTC should be realizable in current

*Contact author: felix.russo@tuwien.ac.at
†Contact author: thomas.pohl@itp.tuwien.ac.at

Published by the American Physical Society under the terms of the Creative Commons Attribution 4.0 International license. Further distribution of this work must maintain attribution to the author(s) and the published article's title, journal citation, and DOI.

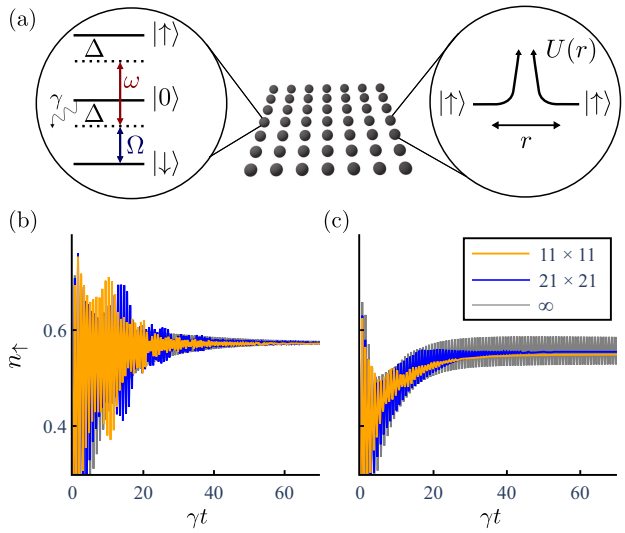


FIG. 1. (a) The three states of spin-1 particles in a two-dimensional lattice are coupled by a resonant field with Rabi frequency ω and a field with Rabi frequency Ω that is detuned by Δ from the lower transition. Dissipation arises from spontaneous decay of the intermediate state with a rate γ. Interactions $U(r)$ cause state-dependent energy shifts for two particles at a distance r. The interplay of coherent coupling, dissipation, and interactions can lead to persistent oscillations. While mean-field theory predicts a stationary steady-state value of the $|\uparrow\rangle$-state population $n_\uparrow$ in the thermodynamic limit for the chosen set of parameters in (b), persistent oscillations emerge upon accounting for beyond-mean-field effects as shown in (c). Such a quantum dissipative time-crystal phase, thus, breaks the continuous time-translational symmetry of the system in the absence of a limit cycle in the classical mean-field dynamics.

quantum simulation experiments with Rydberg atomic arrays.

We consider a two-dimensional cubic lattice of three-level systems with quantum states $|\downarrow\rangle$, $|\uparrow\rangle$, and $|0\rangle$, as illustrated in Fig. 1(a). The intermediate state $|0\rangle$ is coupled to the upper $|\uparrow\rangle$ and lower $|\downarrow\rangle$ states with respective Rabi frequencies ω (resonant) and Ω (Δ detuned). The corresponding Hamiltonian for N such three-level systems can be written as

$$\hat{H} = \Delta \sum_i \hat{n}_\downarrow^{(i)} + \sum_i \left(\Omega \hat{\sigma}_{\downarrow 0}^{(i)} + \omega \hat{\sigma}_{\uparrow 0}^{(i)} + \text{H.c.} \right) + \sum_{i<j} U_{ij} \hat{n}_\uparrow^{(i)} \hat{n}_\uparrow^{(j)}, \tag{1}$$

where $\hat{\sigma}_{\alpha\beta}^{(i)} = |\alpha\rangle_i\langle\beta|$ denote the transition operators for the ith particle, and $\hat{n}_\alpha^{(i)} = \hat{\sigma}_{\alpha\alpha}^{(i)}$ corresponds to the respective excitation density at a given site. The second line in Eq. (1) describes density-density interactions between particles in the uppermost state $|\uparrow\rangle$. We consider power-law potentials $U_{ij} = C_\kappa / r_{ij}^\kappa$, where C_κ is the interaction strength and $r_{ij} = |\mathbf{r}_j - \mathbf{r}_i|$ the distance between two particles i and j at positions $\mathbf{r}_i$ and $\mathbf{r}_j$ in the lattice. We parametrize the interaction strength by the total interaction energy $\chi = \sum_{j\neq 0} U_{0j}$ of the particle at position $\mathbf{r}_0$ in the center of the lattice with all surrounding spins.

This Hamiltonian applies directly to current experiments with neutral-atom arrays [36–42], where $|\downarrow\rangle$ corresponds to an atomic ground state, $|0\rangle$ to a low-lying intermediate state, and $|\uparrow\rangle$ to a highly excited Rydberg state. Laser fields can be used to drive the $|0\rangle \leftrightarrow |\downarrow\rangle$ and $|0\rangle \leftrightarrow |\uparrow\rangle$ transitions with Rabi frequencies Ω and ω, as described by Eq. (1). Considering resonant laser driving of the upper transition, the frequency detuning on the lower transition corresponds to the energy mismatch Δ in Eq. (1). Moreover, Rydberg atoms feature strong van der Waals interactions, $U_{ij} = C_6/r_{ij}^6$ [43–45], while longer-ranged dipole-dipole interactions, $U_{ij} = C_3/r_{ij}^3$, can be realized and controlled via microwave dressing of the Rydberg state [46–48]. While Rydberg states ($|\uparrow\rangle$) typically feature very long lifetimes [43,44,49,50], the radiative decay of the intermediate $|0\rangle$ state introduces dissipation as described by the Lindbladian

$$\hat{\mathcal{L}}(\hat{\rho}) = \gamma \sum_i \left(\hat{\sigma}_{\downarrow 0}^{(i)} \hat{\rho} \hat{\sigma}_{0\downarrow}^{(i)} - \frac{1}{2} \left\{ \hat{n}_0^{(i)}, \hat{\rho} \right\} \right) \tag{2}$$

with a spontaneous decay rate γ. The dynamics of the N-body density matrix $\hat{\rho}$ of the lattice is determined by the quantum master equation

$$\frac{\partial}{\partial t} \hat{\rho} = \mathrm{i}[\hat{\rho}, \hat{H}] + \hat{\mathcal{L}}(\hat{\rho}). \tag{3}$$

Its exact solution can, however, be found numerically only for small particle numbers, such that suitable approximations are required to analyze the nonequilibrium physics of large lattices.

The simplest approach is to entirely neglect correlations by performing a mean-field approximation, which corresponds to the assumption that many-body observables factorize

$$\langle \hat{\sigma}_{\alpha\beta}^{(i)} \hat{\sigma}_{\bar{\alpha}\bar{\beta}}^{(j)} \rangle \approx \sigma_{\alpha\beta}^{(i)} \sigma_{\bar{\alpha}\bar{\beta}}^{(j)}. \tag{4}$$

This approach furnishes a set of coupled mean-field equations for the one-body expectation values $\sigma_{\alpha\beta}^{(i)} = \langle \hat{\sigma}_{\alpha\beta}^{(i)} \rangle$ that can be readily solved and have been used to study steady-state phases in different open quantum systems [19,22,23,26,34,51–56]. In many cases, the nonlinearity that arises from the mean-field interaction can give rise to bistabilities [51,57–59] that can often be related to a first-order nonequilibrium phase transition of the exact quantum dynamics [60]. As pointed out in [26], interacting multilevel systems can also support the formation of nonstationary phases, where the system settles into a state

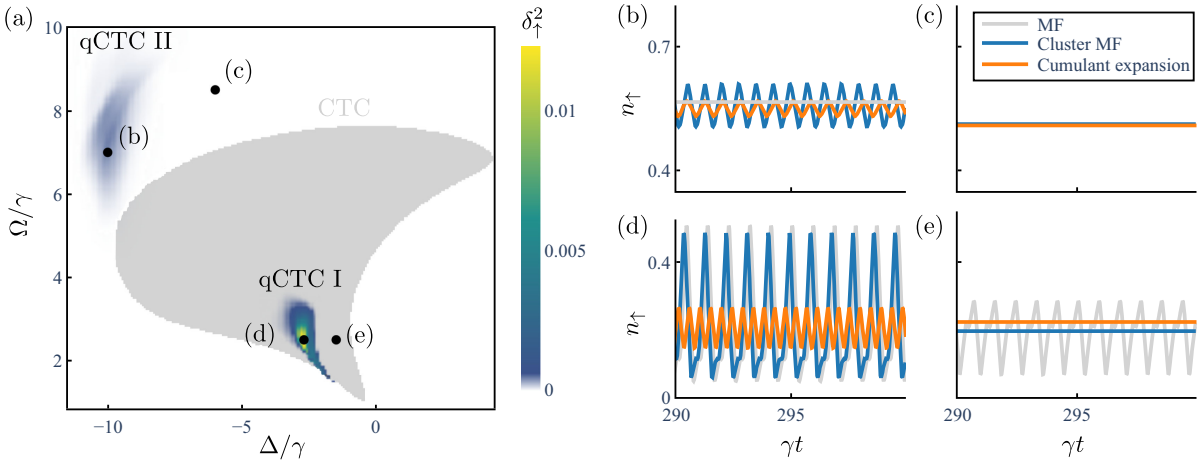


FIG. 2. (a) Phase diagram in the thermodynamic limit for $\omega = 6\gamma$ and $\chi = -18\gamma$. The occurrence of mean-field CTCs is marked by the gray shaded area. The superimposed color map shows the asymptotic oscillation contrast $\delta^2_\uparrow$ [see Eq. (7)] from beyond-mean-field calculations, revealing two distinct oscillatory regions, which we term type-I and type-II qCTC. The qCTC-I phase resides within the mean-field (MF) CTC region, while the mean-field CTC is otherwise damped by beyond-mean-field effects, as illustrated in (d) and (e), respectively. In contrast, time-translational symmetry breaking in the qCTC-II phase occurs outside the classical CTC region and is driven by correlations, as shown in (b) and (c). The oscillation contrast in (a) is obtained from a second-order cumulant expansion, while (b)–(e) compare mean-field dynamics to the results of the cumulant expansion and cluster mean-field simulations described in the text.

with persistent periodic oscillations in the long time limit. Figure 2(a) shows the parameter region where we find such a CTC phase with broken time-translational symmetry from a linear stability analysis of the mean-field equations in the thermodynamic limit (where we can exploit translational invariance) obtained from Eqs. (3) and (4) [61,62]. Indeed, the basic idea of CTC phases in an open quantum many-body system [18] is often based on the validity of mean-field theory. In the present case, this would require $\kappa \leq 2$ such that interactions are long ranged in two dimensions and the mean-field contribution to the interaction dominates in the thermodynamic limit [63].

Consequently, mean-field theory does not straightforwardly apply to the physics of neutral-atom arrays, where relevant interactions, such as van der Waals ($\kappa = 6$) and dipole-dipole ($\kappa = 3$) interactions, are shorter ranged. Various methods have recently been explored [64] to study the dissipative dynamics of quantum many-body systems beyond simplified mean-field models. Here, we employ two complementary approaches to account for correlations in lattices with dipole-dipole interactions ($\kappa = 3$).

First, we use a cumulant expansion that permits a systematic inclusion of correlations through a hierarchy of equations for multiparticle cumulants of increasing order [65–70]. We take second-order correlations into account,

$$\langle \hat{\sigma}^{(i)}_{\alpha\beta} \hat{\sigma}^{(j)}_{\tilde{\alpha}\tilde{\beta}} \rangle = \sigma^{(i)}_{\alpha\beta} \sigma^{(j)}_{\tilde{\alpha}\tilde{\beta}} + \langle \hat{\sigma}^{(i)}_{\alpha\beta} \hat{\sigma}^{(j)}_{\tilde{\alpha}\tilde{\beta}} \rangle_c, \tag{5}$$

but neglect three-particle cumulants to truncate the hierarchy of equations [62]. Second, we perform cluster mean-field simulations [71], whereby the density matrix is factorized

$$\hat{\rho} = \bigotimes_i \hat{\rho}_{\mathcal{C}_i} \tag{6}$$

into finite clusters $\mathcal{C}_i$ of particles. Using this ansatz in the master equation (3), one obtains the exact quantum dynamics on each plaquette $\mathcal{C}_i$, while interactions between particles in different clusters are included on a mean-field level. In the thermodynamic limit, one can assume homogeneity such that all plaquettes become identical, $\hat{\rho}_{\mathcal{C}_i} = \hat{\rho}_{\mathcal{C}}$ [62]. We have performed simulation for 2×2 as well as 3×3 clusters and find very similar results for the parameters of Figs. 2(b)–2(e) (see Supplemental Material [62]).

While either method is approximate, they provide complementary approaches to include quantum fluctuations. In the cumulant expansion, we account only for direct binary correlations but do so for all particle distances throughout the lattice. On the other hand, the cluster mean-field simulations treat correlations only within a finite interaction range but include all orders of correlations via an exact solution of the master equation within a chosen plaquette $\mathcal{C}$. Through this complementarity, the application and comparison of both methods affords more stringent conclusions about the emergence of quantum time-crystalline phases.

In order to detect oscillatory solutions in such simulations we use the time-averaged variance

$$\delta^2_\uparrow = \frac{1}{\tau} \int_t^{t+\tau} n_\uparrow(t')^2 \mathrm{d}t' - \left(\frac{1}{\tau} \int_t^{t+\tau} n_\uparrow(t') \mathrm{d}t' \right)^2 \tag{7}$$

of the Rydberg-state density, $n_\uparrow = N^{-1} \sum_i \langle \hat{n}^{(i)}_\uparrow \rangle$, in the long time limit ($t \to \infty$) and increase τ until $\delta^2_\uparrow$ is

converged. By construction, $\delta^2_\uparrow$ vanishes for stationary steady states and yields a measure of the oscillation amplitude of $n_\uparrow$ in the time-crystal phase.

Figure 2(a) shows how the phase diagram is modified upon including correlations via the second-order cumulant expansion. For most parameters, the boundary time-crystal phase predicted by mean-field theory is expectedly damped upon inclusion of correlations, as illustrated in Fig. 2(e). Remarkably, however, we find a small but finite parameter region where the time-crystalline phase persists in the beyond-mean-field dynamics. We denote this form of quantum time crystals as qCTC-I and have confirmed their existence both via the cumulant expansion and cluster mean-field simulations, as shown in Fig. 2(d) [62]. Surprisingly, we find another time-crystal phase, marked as qCTC-II in Fig. 2(a). This type-II oscillatory solution emerges outside the classical mean-field regime, i.e., in a parameter region where the mean-field solution settles into a stationary steady state [62]. Rather than damping the mean-field dynamics, accounting for correlations causes a breaking of time-translation symmetry. Oscillations in this novel time-crystal phase are thus driven by beyond-mean-field effects, as shown in Fig. 2(b).

For a more detailed analysis of the two qCTC phases, we study the variance

$$\Delta N^2_\uparrow = \langle \hat{N}^2_\uparrow \rangle - \langle \hat{N}_\uparrow \rangle^2, \tag{8}$$

of the total population in the $|\uparrow\rangle$ state, given by $\hat{N}_\uparrow = \sum_i \hat{n}^{(i)}_\uparrow$. For boundary time crystals with all-to-all interactions [18], pertinent to mean-field theory, it was found that fluctuations of the type $F^2 = \Delta N^2_\uparrow / N$ [72–78] grow linearly with the number N of particles while remaining finite for stationary steady states [53]. As shown in Figs. 3(a) and 3(c), this behavior is recovered in the qCTC-I phase of our system. In stark contrast, however, in the qCTC-II phase, we find a sublinear growth of F^2 upon increasing the particle number N. While the observed increase of F^2 still distinguishes the time crystal from the stationary phase, the observed weak power-law dependence $F^2 \sim N^{0.06}$ differs distinctively from the linear mean-field scaling of the qCTC-I time crystal (Supplemental Material [62]). Notably, this implies that the relative uncertainty $\Delta N_\uparrow / N_\uparrow$ approaches a finite value as $N \to \infty$ for the type-I time crystal, while it vanishes in the thermodynamic limit of the qCTC-II phase. This behavior is consistent with the results of [35], where it was shown that persistent oscillations can emerge in quenched isolated quantum many-body systems in the absence of long-range spatial correlations, demonstrating that spatial long-range order is irrelevant for time-translational symmetry breaking.

Despite the sublinear scaling behavior in qCTC-II, quantum fluctuations have a significant effect on the dynamics of the system in either phase, owing to the finite-range nature of the interaction. We can quantify the impact of correlations by comparing the total mean-field interaction energy

$$E_{\mathrm{MF}} = \sum_{i,j>i} U_{ij} n^{(i)}_\uparrow n^{(j)}_\uparrow \tag{9}$$

to the correlation energy

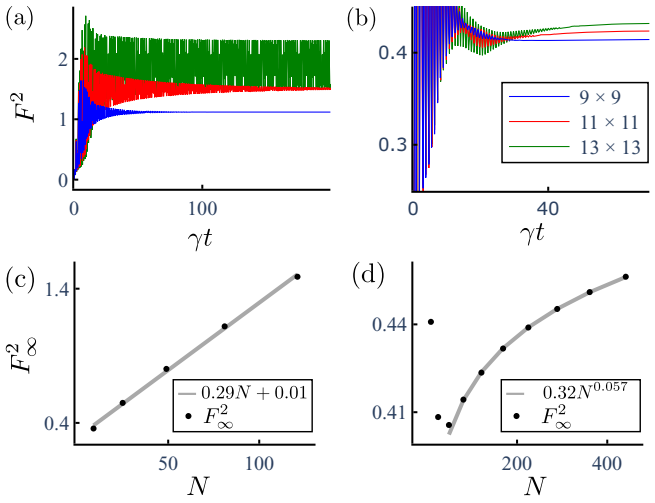


FIG. 3. Dynamics of the normalized variance $F^2 = \Delta N^2_\uparrow / N$ in the (a) qCTC-I and the (b) qCTC-II phase. (c),(d) The corresponding dependence of steady-state value $F^2_\infty = \lim_{t\to\infty} F^2$ on the particle number N. The interaction strength was fixed to $\chi = -18\gamma$ for all system sizes. Fits to a linear (c) and a power law (d) are shown in gray. Since the longer-lived oscillations in qCTC-I prevent reaching a steady state within reasonable simulation times for large systems, we show fewer data points in (c).

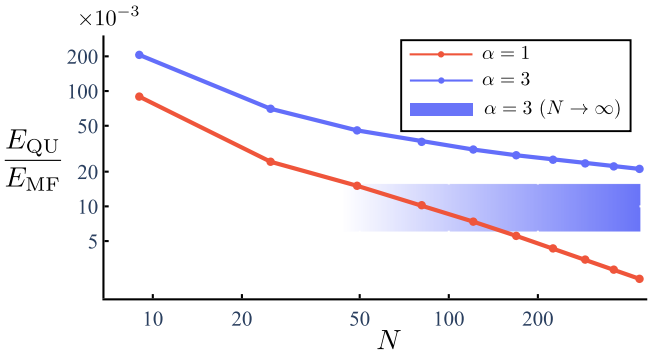


FIG. 4. Ratio between correlation and mean-field energy for a long- ($\kappa = 1$) and short-range ($\kappa = 3$) interaction potential. Parameters are taken from qCTC-II. In the long-range case, the energy ratio tends to 0 as the thermodynamic limit is approached. In the short-range case, on the other hand, the correlations remain non-negligible as $N \to \infty$, and the energy ratio fluctuates between finite values due to the broken time-translation symmetry. The oscillation range in the thermodynamic limit for $\kappa = 3$ is depicted as a blue area. For all system sizes and potentials, the interaction strength was fixed to $\chi = -18\gamma$.

$$E_{\mathrm{QU}} = \sum_{i,j>i} U_{ij} \langle \hat{n}_{\uparrow}^{(i)} \hat{n}_{\uparrow}^{(j)} \rangle_c. \tag{10}$$

As shown in Fig. 4 for the qCTC-II phase, the ratio $E_{\mathrm{QU}}/E_{\mathrm{MF}}$ indeed approaches a finite value in the thermodynamic limit [62]. In contrast, an exact description via mean-field theory requires $E_{\mathrm{QU}}/E_{\mathrm{MF}}$ to vanish in the thermodynamic limit, which is the case for long-range interacting systems [22,23,28,34,53,55]. This is illustrated numerically in Fig. 4 for a long-range interacting lattice with $\kappa = 1$ and otherwise identical parameters. As correlations in open quantum systems can be both of classical and quantum origin, we studied the dynamics of the logarithmic negativity, which provides a measure of entanglement [79]. Indeed, we find finite entanglement in both time-crystal phases [62]. Thus, we conclude that the qCTC-II time-crystal phase can be considered a quantum effect beyond the classical dynamics of dissipative time crystals under mean-field conditions.

In summary, we have studied the dissipative dynamics of interacting three-level quantum systems and found nonequilibrium phases with persistent oscillations that extend the mean-field phenomenology of CTC phases. In particular, we have shown that continuous time-translational symmetry can be broken as a direct consequence of beyond-mean-field effects. Fluctuations in such quantum continuous time crystals (here termed qCTC-II) exhibit distinctly different scaling behavior than found in mean-field models with long-range interactions [53].

The reported dynamics of spin-1 lattices could not be found in equivalent spin-1/2 systems, raising interesting questions regarding the fundamental requirements for the emergence of CTC phases and motivating further explorations of minimal models for qCTCs in many-body systems. Addressing these issues could expand the understanding of the basic mechanisms for CTC formation in open quantum systems, possibly beyond the phenomenology of periodic orbits in classical nonlinear systems, and may yield a suitable classification of distinct time-crystalline phases [80,81]. Moreover, the observation of persistent oscillations in the presence of local decay poses exciting questions concerning the general stability of different time-crystal phases with respect to perturbations and the role of dissipation [82].

Our model applies directly to the physics of neutral-atom arrays [36–42], which should make detailed experimental explorations of the predicted time-crystalline dynamics possible. Here, the qCTC-II phase appears particularly attractive as the intermediate-state population turns out to be very small in the oscillating phase. The type-II time crystal, thus, forms an approximate dark state in which persistent oscillations primarily occur between the $|\downarrow\rangle$ and $|\uparrow\rangle$ state, such that heating of the atoms due to photon emission from the $|0\rangle$ state remains at a low level (Supplemental Material [62]). The parameters considered in this Letter are typical for arrays of rubidium atoms. The considered Rabi frequencies of around $\sim 10\gamma$ correspond to readily achievable values of $\sim$13 MHz for two-photon excitation of nS-Rydberg states via the intermediate $6P$ state [83]. The chosen interaction strength of $\chi = -18\gamma$ would correspond to a modest nearest-neighbor interaction of $C_3/a^3 = -2.6$ MHz, which can be realized experimentally by off-resonant microwave dressing [47] of a $|nS\rangle$-Rydberg state with a $|nP\rangle$ state, enabling a strong resonant dipole-dipole interaction.

Note added—Recently, we became aware of a related work on time-crystal phases in open spin chains with power-law interactions [84].

Acknowledgments—We thank Fan Yang, Klaus Mølmer, Jan Kumlin, Simon P. Pedersen, and Andreas Nunnenkamp for insightful discussions. This work was supported by funding from the Austrian Science Fund (FWF) [Grant DOI: 10.55776/COE1] and the European Union (NextGenerationEU), by the SNSF through the Swiss Quantum Initiative, and from the European Research Council through the ERC Synergy Grant SuperWave (Grant No. 101071882).

Data availability—The data that support the findings of this article are not publicly available. The data are available from the authors upon reasonable request.

[1] F. Strocchi, *Symmetry Breaking* (Springer, New York, 2005), Vol. 643.
[2] F. Wilczek, Quantum time crystals, Phys. Rev. Lett. **109**, 160401 (2012).
[3] K. Sacha and J. Zakrzewski, Time crystals: A review, Rep. Prog. Phys. **81**, 016401 (2017).
[4] P. Hannaford and K. Sacha, A decade of time crystals: Quo vadis?, Europhys. Lett. **139**, 10001 (2022).
[5] M. P. Zaletel, M. Lukin, C. Monroe, C. Nayak, F. Wilczek, and N. Y. Yao, Colloquium: Quantum and classical discrete time crystals, Rev. Mod. Phys. **95**, 031001 (2023).
[6] K. Sacha, Modeling spontaneous breaking of time-translation symmetry, Phys. Rev. A **91**, 033617 (2015).
[7] D. V. Else, B. Bauer, and C. Nayak, Floquet time crystals, Phys. Rev. Lett. **117**, 090402 (2016).
[8] V. Khemani, A. Lazarides, R. Moessner, and S. L. Sondhi, Phase structure of driven quantum systems, Phys. Rev. Lett. **116**, 250401 (2016).
[9] S. Choi, J. Choi, R. Landig, G. Kucsko, H. Zhou, J. Isoya, F. Jelezko, S. Onoda, H. Sumiya, V. Khemani *et al.*, Observation of discrete time-crystalline order in a disordered dipolar many-body system, Nature (London) **543**, 221 (2017).
[10] J. Zhang, P. W. Hess, A. Kyprianidis, P. Becker, A. Lee, J. Smith, G. Pagano, I.-D. Potirniche, A. C. Potter, A. Vishwanath *et al.*, Observation of a discrete time crystal, Nature (London) **543**, 217 (2017).

[11] A. Kyprianidis, F. Machado, W. Morong, P. Becker, K. S. Collins, D. V. Else, L. Feng, P. W. Hess, C. Nayak, G. Pagano *et al.*, Observation of a prethermal discrete time crystal, Science **372**, 1192 (2021).
[12] S. Pal, N. Nishad, T. Mahesh, and G. Sreejith, Temporal order in periodically driven spins in star-shaped clusters, Phys. Rev. Lett. **120**, 180602 (2018).
[13] J. Rovny, R. L. Blum, and S. E. Barrett, Observation of discrete-time-crystal signatures in an ordered dipolar many-body system, Phys. Rev. Lett. **120**, 180603 (2018).
[14] J. O'Sullivan, O. Lunt, C. W. Zollitsch, M. Thewalt, J. J. Morton, and A. Pal, Signatures of discrete time crystalline order in dissipative spin ensembles, New J. Phys. **22**, 085001 (2020).
[15] J. Randall, C. Bradley, F. van der Gronden, A. Galicia, M. Abobeih, M. Markham, D. Twitchen, F. Machado, N. Yao, and T. Taminiau, Many-body–localized discrete time crystal with a programmable spin-based quantum simulator, Science **374**, 1474 (2021).
[16] H. Keßler, P. Kongkhambut, C. Georges, L. Mathey, J. G. Cosme, and A. Hemmerich, Observation of a dissipative time crystal, Phys. Rev. Lett. **127**, 043602 (2021).
[17] A. Greilich, N. E. Kopteva, V. L. Korenev, and M. Bayer, Exploring nonlinear dynamics in periodically driven time crystal: From synchronized to chaotic motion, Nat. Commun. **16**, 2936 (2025).
[18] F. Iemini, A. Russomanno, J. Keeling, M. Schirò, M. Dalmonte, and R. Fazio, Boundary time crystals, Phys. Rev. Lett. **121**, 035301 (2018).
[19] C.-K. Chan, T. E. Lee, and S. Gopalakrishnan, Limit-cycle phase in driven-dissipative spin systems, Phys. Rev. A **91**, 051601(R) (2015).
[20] H. Keßler, J. G. Cosme, M. Hemmerling, L. Mathey, and A. Hemmerich, Emergent limit cycles and time crystal dynamics in an atom-cavity system, Phys. Rev. A **99**, 053605 (2019).
[21] B. Buča, J. Tindall, and D. Jaksch, Non-stationary coherent quantum many-body dynamics through dissipation, Nat. Commun. **10**, 1730 (2019).
[22] P. Kongkhambut, J. Skulte, L. Mathey, J. G. Cosme, A. Hemmerich, and H. Keßler, Observation of a continuous time crystal, Science **377**, 670 (2022).
[23] Y. Li, C. Wang, Y. Tang, and Y.-C. Liu, Time crystal in a single-mode nonlinear cavity, Phys. Rev. Lett. **132**, 183803 (2024).
[24] T. Liu, J.-Y. Ou, K. F. MacDonald, and N. I. Zheludev, Photonic metamaterial analogue of a continuous time crystal, Nat. Phys. **19**, 986 (2023).
[25] K. Wadenpfuhl and C. S. Adams, Emergence of synchronization in a driven-dissipative hot rydberg vapor, Phys. Rev. Lett. **131**, 143002 (2023).
[26] X. Wu, Z. Wang, F. Yang, R. Gao, C. Liang, M. K. Tey, X. Li, T. Pohl, and L. You, Dissipative time crystal in a strongly interacting Rydberg gas, Nat. Phys. **20**, 1389 (2024).
[27] A. Greilich, N. E. Kopteva, A. N. Kamenskii, P. S. Sokolov, V. L. Korenev, and M. Bayer, Robust continuous time crystal in an electron–nuclear spin system, Nat. Phys. **20**, 631 (2024).
[28] B. Zhu, J. Marino, N. Y. Yao, M. D. Lukin, and E. A. Demler, Dicke time crystals in driven-dissipative quantum many-body systems, New J. Phys. **21**, 073028 (2019).
[29] A. Pizzi, A. Nunnenkamp, and J. Knolle, Classical prethermal phases of matter, Phys. Rev. Lett. **127**, 140602 (2021).
[30] B. Ye, F. Machado, and N. Y. Yao, Floquet phases of matter via classical prethermalization, Phys. Rev. Lett. **127**, 140603 (2021).
[31] A. Pizzi, A. Nunnenkamp, and J. Knolle, Classical approaches to prethermal discrete time crystals in one, two, and three dimensions, Phys. Rev. B **104**, 094308 (2021).
[32] P. Solanki, A. Cabot, M. Brunelli, F. Carollo, C. Bruder, and I. Lesanovsky, Generation of entanglement and non-stationary states via competing coherent and incoherent bosonic hopping, arXiv:2501.09790.
[33] S. Dutta, S. Zhang, and M. Haque, Quantum origin of limit cycles, fixed points, and critical slowing down, Phys. Rev. Lett. **134**, 050407 (2025).
[34] E. T. Owen, J. Jin, D. Rossini, R. Fazio, and M. J. Hartmann, Quantum correlations and limit cycles in the driven-dissipative Heisenberg lattice, New J. Phys. **20**, 045004 (2018).
[35] M. Medenjak, B. Buča, and D. Jaksch, Isolated Heisenberg magnet as a quantum time crystal, Phys. Rev. B **102**, 041117 (R) (2020).
[36] H. Labuhn, D. Barredo, S. Ravets, S. de Léséleuc, T. Macrì, T. Lahaye, and A. Browaeys, Tunable two-dimensional arrays of single Rydberg atoms for realizing quantum Ising models, Nature (London) **534**, 667 (2016).
[37] H. Bernien, S. Schwartz, A. Keesling, H. Levine, A. Omran, H. Pichler, S. Choi, A. S. Zibrov, M. Endres, M. Greiner *et al.*, Probing many-body dynamics on a 51-atom quantum simulator, Nature (London) **551**, 579 (2017).
[38] P. Scholl, M. Schuler, H. J. Williams, A. A. Eberharter, D. Barredo, K.-N. Schymik, V. Lienhard, L.-P. Henry, T. C. Lang, T. Lahaye, A. M. Läuchli, and A. Browaeys, Quantum simulation of 2d antiferromagnets with hundreds of Rydberg atoms, Nature (London) **595**, 233 (2021).
[39] A. Browaeys and T. Lahaye, Many-body physics with individually controlled Rydberg atoms, Nat. Phys. **16**, 132 (2020).
[40] A. M. Kaufman and K.-K. Ni, Quantum science with optical tweezer arrays of ultracold atoms and molecules, Nat. Phys. **17**, 1324 (2021).
[41] K. Srakaew, P. Weckesser, S. Hollerith, D. Wei, D. Adler, I. Bloch, and J. Zeiher, A subwavelength atomic array switched by a single Rydberg atom, Nat. Phys. **19**, 714 (2023).
[42] P. Weckesser, K. Srakaew, T. Blatz, D. Wei, D. Adler, S. Agrawal, A. Bohrdt, I. Bloch, and J. Zeiher, Realization of a Rydberg-dressed extended Bose Hubbard model, arXiv:2405.20128.
[43] T. F. Gallagher, Rydberg atoms, in *Springer Handbook of Atomic, Molecular, and Optical Physics* (Springer, New York, 1994), pp. 231–240.
[44] M. Saffman, T. G. Walker, and K. Mølmer, Quantum information with Rydberg atoms, Rev. Mod. Phys. **82**, 2313 (2010).

[45] S. Weber, C. Tresp, H. Menke, A. Urvoy, O. Firstenberg, H. P. Büchler, and S. Hofferberth, Calculation of Rydberg interaction potentials, J. Phys. B **50**, 133001 (2017).
[46] M. Tanasittikosol, J. Pritchard, D. Maxwell, A. Gauguet, K. Weatherill, R. Potvliege, and C. Adams, Microwave dressing of Rydberg dark states, J. Phys. B **44**, 184020 (2011).
[47] S. Sevinçli and T. Pohl, Microwave control of Rydberg atom interactions, New J. Phys. **16**, 123036 (2014).
[48] D. Kurdak, P. R. Banner, Y. Li, S. R. Muleady, A. V. Gorshkov, S. Rolston, and J. Porto, Enhancement of Rydberg blockade via microwave dressing, Phys. Rev. Lett. **134**, 123404 (2025).
[49] R. Löw, H. Weimer, J. Nipper, J. B. Balewski, B. Butscher, H. P. Büchler, and T. Pfau, An experimental and theoretical guide to strongly interacting Rydberg gases, J. Phys. B **45**, 113001 (2012).
[50] M. Morgado and S. Whitlock, Quantum simulation and computing with Rydberg-interacting qubits, AVS Quantum Sci. **3** (2021).
[51] T. E. Lee, H. Häffner, and M. C. Cross, Antiferromagnetic phase transition in a nonequilibrium lattice of Rydberg atoms, Phys. Rev. A **84**, 031402(R) (2011).
[52] M. Marcuzzi, E. Levi, S. Diehl, J. P. Garrahan, and I. Lesanovsky, Universal nonequilibrium properties of dissipative Rydberg gases, Phys. Rev. Lett. **113**, 210401 (2014).
[53] F. Carollo and I. Lesanovsky, Exact solution of a boundary time-crystal phase transition: Time-translation symmetry breaking and non-Markovian dynamics of correlations, Phys. Rev. A **105**, L040202 (2022).
[54] P. Solanki, M. Krishna, M. Hajdušek, C. Bruder, and S. Vinjanampathy, Exotic synchronization in continuous time crystals outside the symmetric subspace, Phys. Rev. Lett. **133**, 260403 (2024).
[55] T. Nadolny, C. Bruder, and M. Brunelli, Nonreciprocal synchronization of active quantum spins, Phys. Rev. X **15**, 011010 (2025).
[56] S. Yang, Z. Wang, L. Fu, and J. Jie, Emergent continuous time crystal in dissipative quantum spin system without driving, Commun. Phys. **8**, 114 (2025).
[57] C. Carr, R. Ritter, C. G. Wade, C. S. Adams, and K. J. Weatherill, Nonequilibrium phase transition in a dilute Rydberg ensemble, Phys. Rev. Lett. **111**, 113901 (2013).
[58] N. R. De Melo, C. G. Wade, N. Šibalić, J. M. Kondo, C. S. Adams, and K. J. Weatherill, Intrinsic optical bistability in a strongly driven Rydberg ensemble, Phys. Rev. A **93**, 063863 (2016).
[59] N. Šibalić, C. G. Wade, C. S. Adams, K. J. Weatherill, and T. Pohl, Driven-dissipative many-body systems with mixed power-law interactions: Bistabilities and temperature-driven nonequilibrium phase transitions, Phys. Rev. A **94**, 011401(R) (2016).
[60] H. Weimer, Variational principle for steady states of dissipative quantum many-body systems, Phys. Rev. Lett. **114**, 040402 (2015).
[61] S. H. Strogatz, *Nonlinear Dynamics and Chaos with Student Solutions Manual: With Applications to Physics, Biology, Chemistry, and Engineering* (Westview Press, Cambridge, MA, 2018).
[62] See Supplemental Material at http://link.aps.org/supplemental/10.1103/dc2s-94gv for details on the cumulant expansion and the cluster mean-field simulations, a discussion of energies and fluctuations in the thermodynamic limit, a comparison of the beyond-mean-field spectra, an analysis of atom heating due to spontaneous photon emission, a calculation of an entanglement measure, an explication of the linear stability analysis, and a confirmation of the absence of a mean-field limit cycle in the qCTC-II parameter regime.
[63] R. Mattes, I. Lesanovsky, and F. Carollo, Long-range interacting systems are locally noninteracting, Phys. Rev. Lett. **134**, 070402 (2025).
[64] H. Weimer, A. Kshetrimayum, and R. Orús, Simulation methods for open quantum many-body systems, Rev. Mod. Phys. **93**, 015008 (2021).
[65] R. Kubo, Generalized cumulant expansion method, J. Phys. Soc. Jpn. **17**, 1100 (1962).
[66] F. Lackner, I. Březinová, T. Sato, K. L. Ishikawa, and J. Burgdörfer, High-harmonic spectra from time-dependent two-particle reduced-density-matrix theory, Phys. Rev. A **95**, 033414 (2017).
[67] D. Plankensteiner, C. Hotter, and H. Ritsch, Quantum-Cumulants.jl: A Julia framework for generalized mean-field equations in open quantum systems, Quantum **6**, 617 (2022).
[68] S. Donsa, F. Lackner, J. Burgdörfer, M. Bonitz, B. Kloss, A. Rubio, and I. Březinová, Nonequilibrium correlation dynamics in the one-dimensional Fermi-Hubbard model: A testbed for the two-particle reduced density matrix theory, Phys. Rev. Res. **5**, 033022 (2023).
[69] W. Verstraelen, D. Huybrechts, T. Roscilde, and M. Wouters, Quantum and classical correlations in open quantum spin lattices via truncated-cumulant trajectories, PRX Quantum **4**, 030304 (2023).
[70] K. J. Kusmierek, S. Mahmoodian, M. Cordier, J. Hinney, A. Rauschenbeutel, M. Schemmer, P. Schneeweiss, J. Volz, and K. Hammerer, Higher-order mean-field theory of chiral waveguide QED, SciPost Phys. Core **6**, 041 (2023).
[71] J. Jin, A. Biella, O. Viyuela, L. Mazza, J. Keeling, R. Fazio, and D. Rossini, Cluster mean-field approach to the steady-state phase diagram of dissipative spin systems, Phys. Rev. X **6**, 031011 (2016).
[72] F. Benatti, F. Carollo, R. Floreanini, and H. Narnhofer, Quantum spin chain dissipative mean-field dynamics, J. Phys. A **51**, 325001 (2018).
[73] D. Goderis and P. Vets, Central limit theorem for mixing quantum systems and the CCR-algebra of fluctuations, Commun. Math. Phys. **122**, 249 (1989).
[74] D. Goderis, A. Verbeure, and P. Vets, Non-commutative central limits, Probab. Theory Related Fields **82**, 527 (1989).
[75] D. Goderis, A. Verbeure, and P. Vets, Dynamics of fluctuations for quantum lattice systems, Commun. Math. Phys. **128**, 533 (1990).
[76] A. F. Verbeure, *Many-Body Boson Systems: Half a Century Later* (Springer, New York, 2010).
[77] F. Benatti, F. Carollo, R. Floreanini, and H. Narnhofer, Non-Markovian mesoscopic dissipative dynamics of open quantum spin chains, Phys. Lett. A **380**, 381 (2016).

[78] F. Benatti, F. Carollo, R. Floreanini, and H. Narnhofer, Quantum fluctuations in mesoscopic systems, J. Phys. A **50**, 423001 (2017).

[79] G. Vidal and R. F. Werner, Computable measure of entanglement, Phys. Rev. A **65**, 032314 (2002).

[80] L. M. Sieberer, M. Buchhold, J. Marino, and S. Diehl, Universality in driven open quantum matter, Rev. Mod. Phys. **97**, 025004 (2025).

[81] R. Daviet, C. P. Zelle, A. Asadollahi, and S. Diehl, Kardar-Parisi-Zhang scaling in time-crystalline matter, Phys. Rev. Lett. **135**, 047101 (2025).

[82] R. Yousefjani, A. Carollo, K. Sacha, S. Al-Kuwari, and A. Bayat, Non-Hermitian discrete time crystals, arXiv: 2410.22713.

[83] H. Levine, A. Keesling, A. Omran, H. Bernien, S. Schwartz, A. S. Zibrov, M. Endres, M. Greiner, V. Vuletić, and M. D. Lukin, High-fidelity control and entanglement of Rydberg-atom qubits, Phys. Rev. Lett. **121**, 123603 (2018).

[84] Z. Wang, R. Gao, X. Wu, B. Buča, K. Mølmer, L. You, and F. Yang, Boundary time crystals induced by local dissipation and long-range interactions, arXiv:2503.20761.